International Conference on Engineering and Technology (ICET) - Local Conference

First-Principles Simulation on Orientation Dependence of Piezoresistivity in Graphene Nanoribbon

Mohammed Gamil[1,2,*], Koichi Nakamura[1,3], Ahmed M.R. Fath El-Bab[4,5], Osamu Tabata[2], Ahmed Abd El-Moneim[1,6]

[1]Materials Science and Engineering Department (MSE), Egypt-Japan University of Science and Technology (E-JUST), Alexandria, Egypt, Mohamed.gamil@ejust.edu.eg

[2]Department of Micro Engineering, Kyoto University, Kyoto, Japan, tabata@me.kyoto-u.ac.jp

[3]Center for the Promotion of Interdisciplinary Education and Research, Kyoto University, Kyoto, Japan, koichi@cpier.kyoto-u.ac.jp

[4]Mechatronics and Robotics Department, Egypt-Japan University of Science and Technology, Alexandria, Egypt

[5]On-leave from Mechanical Engineering Department, Faculty of Engineering, Assiut University, Assiut, Egypt, ahmed.rashad@ejust.edu.eg

[6]On leave from Physical Chemistry Department, National Research Center, Cairo, Egypt, ahmed.abdelmoneim@ejust.edu.eg

***Abstract*— The orientation dependence of piezoresistivity in graphene nanoribbons has been discussed by carrying out the first-principles simulation. Our original procedure of simulating piezoresistive properties was applied to the one-dimensional nanoribbon systems in conductor state. For the armchair-oriented model series, band structures hardly change due to any strain, and the gauge factors are small as the common characteristics for the armchair-oriented graphene nanoribbons. On the other hand, various values of gauge factors have been obtained according to model size for the zigzag model series because of the nonuniformity of band structures among the model series. Generally, the zigzag model series have sufficiently large values of gauge factors for practical application to nanoscale piezoresistor. We have found the clear defference of gauge factors with respect to the orientation of graphene nanoribbon, and it is expected that zigzag-oriented graphene nanoribbons will have potential for use in future MEMS/NEMS technology.**

***Keywords*—graphene, piezoresistivity, gauge factor, first-principles calculation, band energy diagram**

I. INTRODUCTION

Strain measurement is very important in numerous applications in mechanical engineering. So, strain gauges are widely used for this purpose. The strain gauge is a resistance-based sensor that changes its resistance with strain when stretched within its elastic limit [1]. The basic fundamental of the resistance-change in strain gauges is due to geometrical or piezoresistivity change [2]. The sensitivity of the strain gauge, which is highly demanded, can be measured by the gauge factor which results from dividing the relative change of the stretched resistance to the applied mechanical strain [3].

Metallic foil strain gauges were first used for measuring strain, its measurement technique depends mainly on the geometrical change and results in a gauge factor up to 2.1 [4]. The gauge factor of the metallic foil strain gauges is still small and does not fulfill the requirements of the developed sensitive applications. So, many approaches were investigated to obtain higher gauge factor.

Piezoresistivity change is an important factor that can be considered as another source for increasing the gauge factor [4]. Semiconductors like silicon is considered as one of the most widely used piezoresistive material that depends mainly on the piezoresistivity-change due to strain effect, its gauge factor can be reached to 200 depending on the orientation and the doping elements [5]. However, silicon has a lot of constraints that makes it restricted for many applications that needs flexibility. Moreover, the fabrication cost of piezoresistive based-silicon strain gauge is very high due to the ion implantation.

Graphene is a flat monolayer of sp^2 carbon (C) atoms tightly packed together into a two-dimensional (2D) honeycomb lattice as illustrated in Fig. 1 [6]. Graphene is a promising piezoresistive material for strain gauge applications due to its piezoresistivity. In this regard, Lee *et al*. reported in their study that the gauge factor of graphene prepared by chemical vapor deposition over a silicon chip is 6.1 [7], which is small and doesn't fulfill the requirements of the highly sensitive sensors. Meanwhile, Chen *et al*. also reported that the gauge factor of the mechanically exfoliated graphene over a silicon chip is ranging from 10 to 15 depending on the number of laers [8]. Although, the gauge factor is high, the method is low yield, messy, non-reproducible and time consuming process which is limited to small scale production. The need of flexible strain gauge sensors with high sensitivity for the modern high sensitive applications like strain gauges is considered as an urgent demand for the development of these devices.

We have started the simulation of strain gauge factors for a few graphene ribbon models on the basis of first-principles calculation [9]. In this work, we increased graphene ribbon models to discuss the orientation

978-1-4799-5807-8/14/$31.00 @2014 IEEE

dependence of piezoresistivity systematically and evaluated gauge factors for the armchair and zigzag orientation model series according to our original procedure [10, 11] by using another level of first-principles calculation.

II. METHOD OF CALCULATION

A. *First-principles calculation*

First-principles calculations of the periodic boundary models for graphene ribbon have been carried out by VASP program package [12, 13] based on the density functional theory (DFT) [14]. For the DFT exchange-correlation interaction, the generalized-gradient approximation (GGA) method was used by Perdew-Wang (PW91) functionals [15, 16]. We adopted the three dimensional supercell approximation technique with ultrasoft pseudo-potentials prepared according to Vanderbilt [17].

B. *Modeling of graphene ribbon model series*

Zigzag and armchair models have been defined as shown in Fig. 2, where these models have been devised by cutting out a fragment with a one dimensional periodic boundary, and all dangling bonds of C atoms were terminated with hydrogen (H) atoms. The direction of the fragment which is parallel to the *y* direction can be defined as the longitudinal direction, while the parallel to the *x* direction can be considered as the transverse direction as illustrated in Figure 2(c). To represent graphene ribbons, the vacuum space about 5 Å along *x* direction was considered, and then three-dimensional periodic boundary condition was applied. The optimized length of C–C length of strain-free graphene sheet and the Poisson's ratios with respect to the strain along X and Y directions shown in Fig. 1 were referred to from our previous paper [9] as 1.422 Å, 0.14, and 0.28, respectively, for devising strain-free and 1% strained graphene ribbon models. These values are valid as compared with experimental measured C–C length [18] and Poisson's ratios [19-21]. All the structural parameters of the graphene ribbon models such number of C atoms (N_C), number of H atoms (N_H), and the model dimensions are tabulated in Table I.

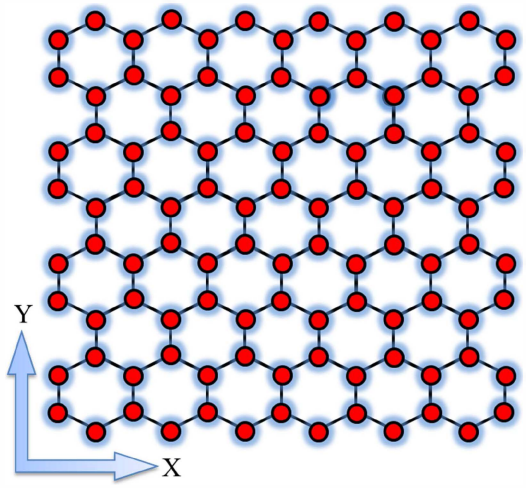

Figure 1. Graphene Sheet.

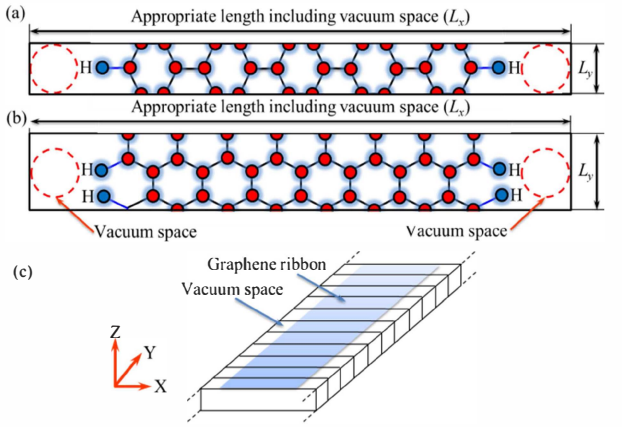

Figure 2. Top views of (a) armchair model (9 rings) and (b) zigzag model (13 rings), and (c) 3D-dimensional periodic boundary condition for these models

III. RESULTS AND DISCUSSION

A. *Band structures of armchair model series*

DFT band strucuture calculations of graphene nanoribbon have been carried out by some research groups [22, 23]. In this work, strain responses of the band structures of graphene ribbon have been investigated with using 1% longitudinal and transverse strained models. The band energy diagrams of the 9-ring and 13-ring armchair models are shown in Figs. 3 and 4, respectively. The valence band (blue lines) maximizes and the conduction band (red lines) minimizes at the Y point, boundary along the longitidunal axis (k_y) between Brillouin zones, respectively. The highest subband of the valence band and the lowest subband of the conduction band approach each other asymptotically as k_y changes toward the Y point, and they are in double degeneracy near the Y point in the vicinity of the Fermi energy. This feature can be also derived by the simple Hückel method qualitatively for the armchair models, and the π orbitals of 9-ring and 13-ring armchair models for the degenerate subbands at the Y point closely resemble each other as shown in Fig. 5. As the common characteristic of the armchair models, the π orbitals of all of armchair models are localized at the edges of graphene ribbon, and no conductance path exists in the center of graphene ribbon. The interaction due to π orbitals along the longitudinal direction is very small because of the non-bonding state due to the antisymmetric relation for the translation with the phase factor $e^{i\pi y/Ly}$, and accordingly, the band energy variation of these degenerate subbands with respect to k point is quite small near the Y point. As a result, low conductivity with heavy effective mass can be explained by using the band orbital interaction.

As it is clear from the band energy diagrams of the strained models, the degenerate subbands in the vicinity of the Fermi energy are not lifted by the longitudinal or transverse strain effect for both of 9-ring and 13-ring models, and the feature of conductivity based on the band energy diagram will not change at all. These features are in good agreement with quite small band orbital interaction as shown in Fig. 5.

TABLE I. STRACTURAL PARAMETERS OF GRAPHENE MODELS

Model Type		(N_C)	(N_H)	Model Dimensions (A°)				
				L_X (Fixed)	L_Y			L_Z (Fixed)
					Strain free	Longitudinal strain	Transvers strain	
Armchair Model	9-Rings	20	2	27.108	2.463	2.487	2.459	10.000
	13-Rings	28		35.640				
Zigzag Model	9-Rings	38	4	29.072	4.266	4.308	4.259	
	11-Rings	46		33.997				
	13-Rings	54		38.924				

B. *Band structures of zigzag model series*

Figs. 6-8 represent the strain responses of the band energy diagrams for the 9-ring, 11-ring, and 13-ring zigzag models, respectively. The valence band maximizes and the conduction band minimizes near the Γ point, respectively. Completely contrary to the armchair model series, we found clear differences of detailed structure of band energy diagram among zigzag model series due to model size; for examples, some zigzag models have small band gaps, and other zigzag models do not have band gaps. This result is consistent with reports by other research groups [22, 23]. In addition, the variation of band energy diagrams of the zigzag model series by the strain is much more sensitive as compared with the armchair model series. In particular, the characteristics of valence-band top and conduction-band bottom subbands near the Fermi energy are caused by both of the longitudinal and transverse strains. Actually, the π orbitals of valence-band top and conduction-band bottom are delocalized, and the band orbital interaction is easy to be caused due to strains.

C. *Evaluation of strain gauge factors*

The electrical conductivity tensor **G** or the electrical resistivity tensor $\boldsymbol{\rho}$ can be represented in terms of carrier density and effective mass tensor by the conventional treatment [24]. Variations of band structure will exert an influence on them, and frequently contribute to a sudden turn of the conductivity. In this paper, we have introduced the band carrier densities for conductive state. The conductivity tensor has been represented as,

$$\mathbf{G} = \boldsymbol{\rho}^{-1} = e^2 \sum_j n_j \boldsymbol{\tau}_j (\mathbf{m}_j^*)^{-1}, \quad (1)$$

where n_j is the jth conduction band carrier electron area density, $\mathbf{m}^*_j$ is the band effective mass tensor, τ_j is the relaxation time tensor, and e^2 is the square of the absolute value of the elementary electric charge. The band carrier densities n_j are defined with the Fermi energy E_F and temperature T;

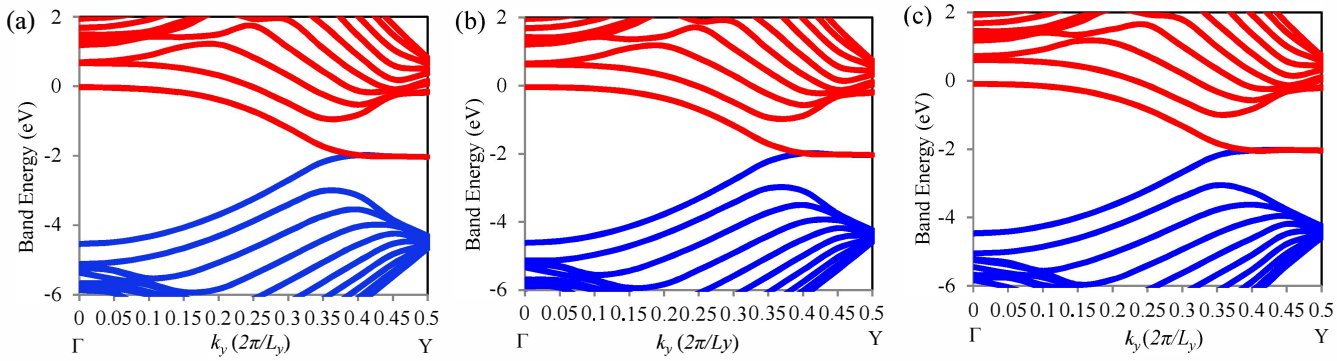

Figure 3. Band energy diagrams for armchair 9-ring armchair (a) no strain model (b) longitudinal strain model (c) transverse strain model.

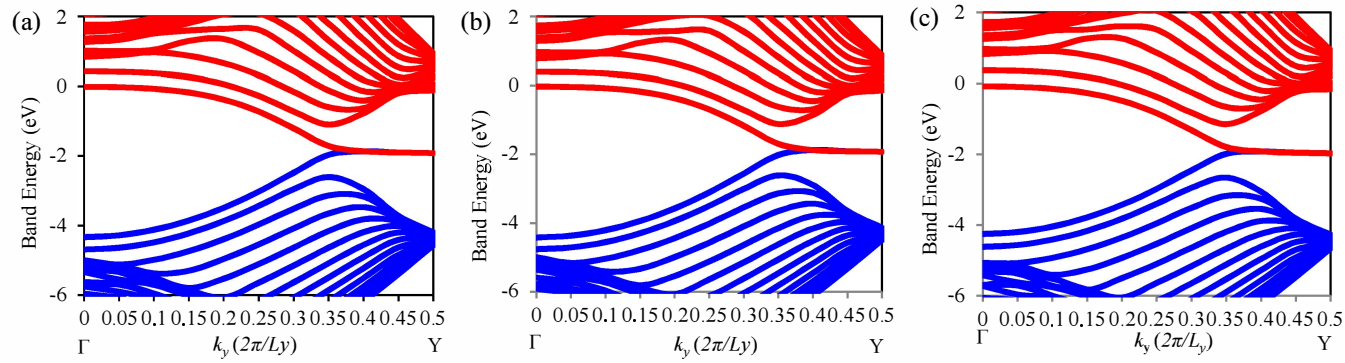

Figure 4. Band energy diagrams for armchair 13-ring armchair (a) no strain model (b) longitudinal strain model (c) transverse strain model.

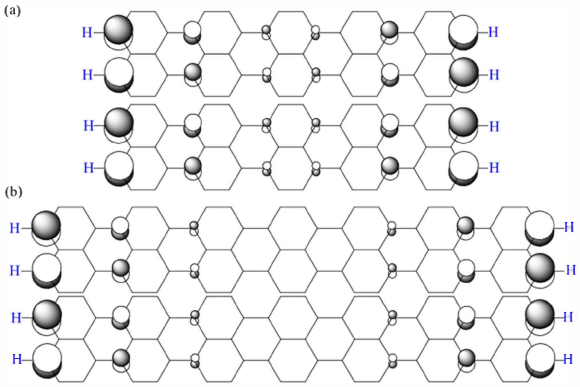

Figure 5. Degenerate p orbitals at Y point near the Fermi energy for the (a) 9-ring and (b) 13-ring armchair models with 2 unit cells.

$$n_j = \frac{2}{S}\int dk_y\, H\left(E_j(k_y) - E_F\right)\left[\exp\left(\frac{E_j(k_y) - E_F}{k_B T}\right)+1\right]^{-1}, \quad (2)$$

where S is the surface area of the graphene model ($S = L_x \times L_y$), $H(E_j(k_y) - E_F)$ is the Heaviside step function with respect to the band dispersion of jth subband $E_j(k_y)$, and k_B is the Boltzmann constant. By using the calculated band energy of the jth subband and k-point weight, $E_{j,ky}$ and w_{ky}, n_j can be approximated as

$$n_j = \frac{2}{S}\sum_{\substack{k_y \\ E_{j,ky} > E_F}} w_{k_y}\left[\exp\left(\frac{E_{j,k_y} - E_F}{k_B T}\right)+1\right]^{-1}. \quad (3)$$

The value of E_F can be solved easily with the total number of valence electrons in the model as follows,

$$N = 4N_C + N_H = 2\sum_j\sum_{k_y} w_{k_y}\left[\exp\left(\frac{E_{j,k_y} - E_F}{k_B T}\right)+1\right]^{-1}. \quad (4)$$

We have performed a sampling with 11 k_y points along the Γ–Y path. The effective mass is generally a 3 × 3 tensor, and the reciprocal matrix of effective mass is defined as [25]

$$(\mathbf{m}^*)^{-1} = \frac{1}{\hbar^2}\begin{pmatrix} \frac{\partial^2 E}{\partial k_x^2} & \frac{\partial^2 E}{\partial k_x \partial k_y} & \frac{\partial^2 E}{\partial k_x \partial k_z} \\ \frac{\partial^2 E}{\partial k_y \partial k_x} & \frac{\partial^2 E}{\partial k_y^2} & \frac{\partial^2 E}{\partial k_y \partial k_z} \\ \frac{\partial^2 E}{\partial k_z \partial k_x} & \frac{\partial^2 E}{\partial k_z \partial k_y} & \frac{\partial^2 E}{\partial k_z^2} \end{pmatrix}, \quad (5)$$

where E is the band energy and $\hbar$ is equal to Planck's constant divided by 2π. The band energies of our graphene models remain constant along the transverse directions, namely,

$$\frac{\partial E}{\partial k_x} = \frac{\partial E}{\partial k_z} = 0, \quad (6)$$

and therefore, the band effective mass of the jth band for the graphene models can be defined simply as a scalar,

$$m_j^* = \hbar^2\left(\frac{\partial^2 E_j}{\partial k_y^2}\right)^{-1}. \quad (7)$$

In this paper, the second derivative on the right hand of (7) has been estimated numerically as

$$\frac{\partial^2 E_j[k_y]}{\partial k_y^2} = \frac{E_j[k_y + \Delta k_y] + E_j[k_y - \Delta k_y] - 2E_j[k_y]}{(\Delta k_y)^2} \quad (8)$$

with $\Delta ky = 0.05\times(2\pi/Ly)$. For the relaxation time in graphene systems, we have introduced the approximation that all of the band relaxation times are equal and constant regardless of stress [10, 11, 26-29]. This procedure seems to be rough to some extent, but the variation rate of carrier conductivity can be easily and adequately represented in consideration of the canceling of almost part of band relaxation times. As a result, the resistivity tensor, inverse of the conductivity tensor, can be also obtained as a scalar, R.

Gauge factor can be defined as,

$$K_\alpha = \frac{R_\alpha - R_0}{R_0}\cdot\frac{1}{\varepsilon_\alpha}, \quad (9)$$

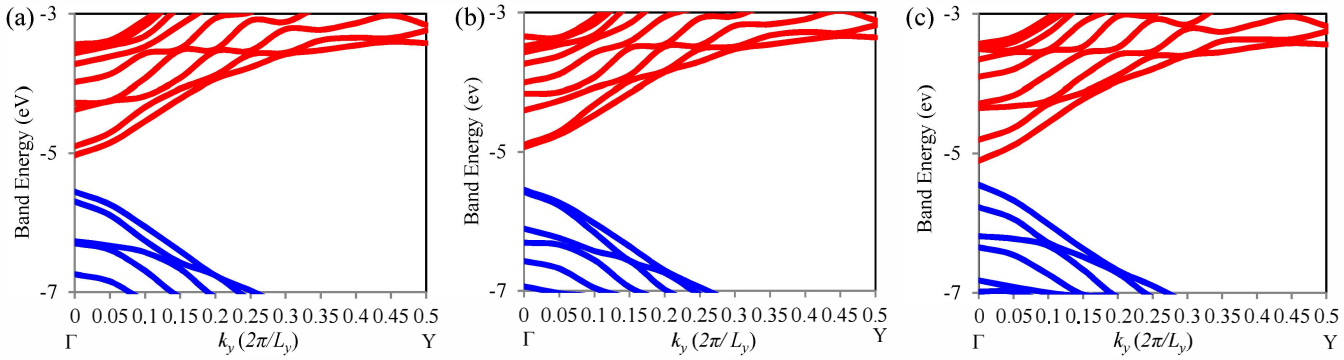

Figure 6. Band energy diagrams for armchair 9-ring zigzag (a) no strain model (b) longitudinal strain model (c) transverse strain model.

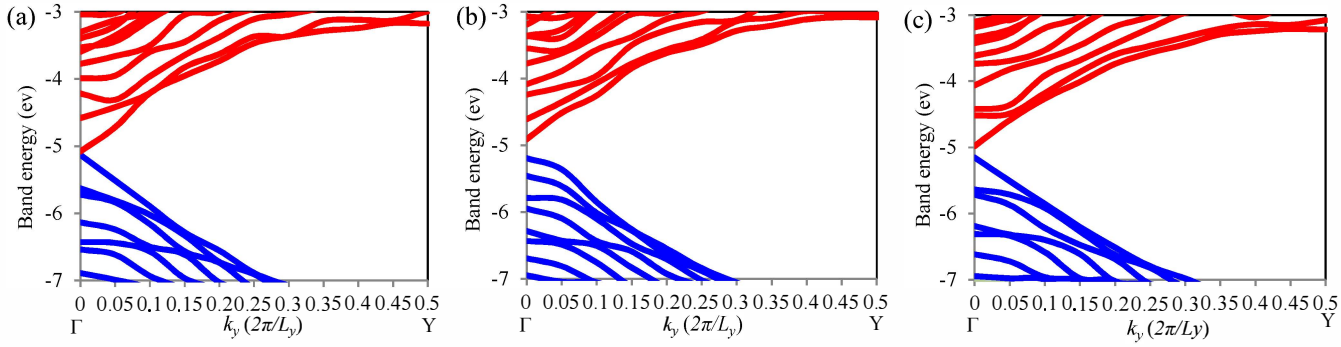

Figure 7. Band energy diagrams for armchair 11-ring zigzag (a) no strain model (b) longitudinal strain model (c) transverse strain model.

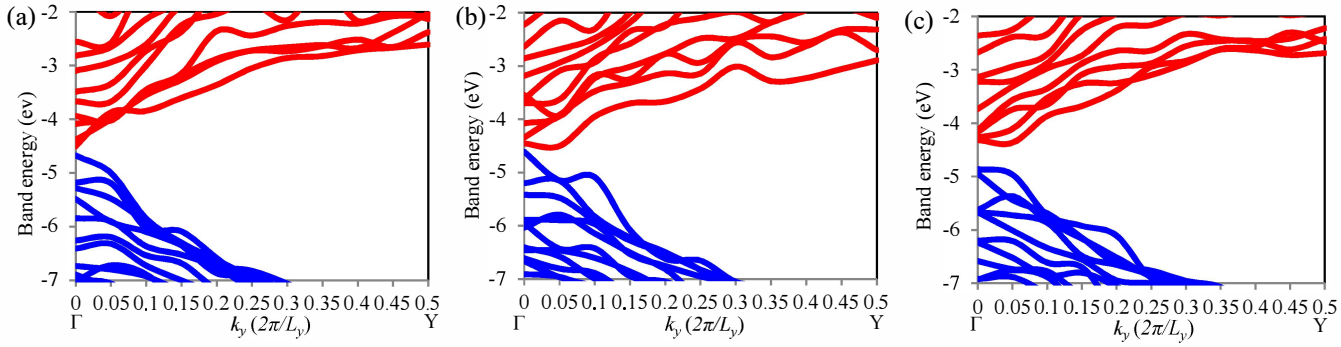

Figure 8. Band energy diagrams for armchair 13-ring zigzag (a) no strain model (b) longitudinal strain model (c) transverse strain model.

where R_α and R_0 are the graphene resistances at applied strain ε_α (α denotes longitudinal or transverse) and at no strain, respectively. From (1) and (9), the gauge factor equation can be written as follows:

$$K_\alpha = \frac{1}{\varepsilon_\alpha}\left(\frac{\sum_j (n_{j,0}/m^*_{j,0})}{\sum_j (n_{j,\alpha}/m^*_{j,\alpha})} - 1\right), \qquad (10)$$

Using the data obtained from the energy diagrams which are tabulated in TABLE II, we can calculate the values of the gauge factors for armchair and zigzag model series as shown in TABLE III.

For the armchair model series, the mobility of carrier is very small regardless of strains because of heavy effective mass, and the band carrier electron area densities do not change due to any strains. As a result, the gauge factors are not so high, and we can conclude that the low piezoresistivity in the armchair model series is the common characteristics for the armchair-oriented graphene nanoribbons.

On the other hand, the zigzag model series have high mobility of carrier due to small effective mass. Actually, for the zigzag models, the energy curves of valence-band top and conduction-band bottom subbands near the Fermi energy are almost linear with respect to k_y, leading to zero effective mass for electrons and holes. This character is clearly corresponding to the conical dispersion relation for general 2D graphene sheet obserbed at the six corners of the 2D Brillouin zone. Therefore, the zigzag ribbon model series keep high conductivity similarly as 2D graphene sheet, and the zigzag-oriented graphene nanoribbons will be applied to nanoscale MEMS/NEMS sensing elements with high conductivity if they can be fabricated selectively under the orieantation control in future. From the viewpoint of piezoresistivity, various values of gauge factors have been obtained in our simulation for the zigzag model series, because the band structures of the zigzag model series are clearly less uniform than those of armchair model series. The change of carrier mobility due to strain gives the result that zigzag model series generally have larger absolute values of gauge factors than the armchair model series. Thus, we have found clear difference in the conductive and piezoresitive characteristics between the armchair and zigzag model series. In particular, the simulated gauge factors for some zigzag models can be regarded as sufficient values for practical application to nanoscale piezoresistor. The systematic piezoresistivity in the zigzag model series will be discussed with additional models and simulation in a continuing research.

TABLE II. PROPRTIES OF THE GRAPHENE MODELRS.

Model Type		E_F (eV)	$\sum_j n_j$ (Cm^{-1})	$(m^*_j/m^{a)}_0)^{-1}$
Armchair Model 9-Rings	Strain-Free	-2.008	2.996×10^{18}	0.071
	Longitudinal Strain	-2.031	2.999×10^{18}	0.068
	Transvers Strain	-2.011	3.003×10^{18}	0.066
Armchair Model 13-Rings	Strain-Free	-1.890	2.283×10^{18}	0.070
	Longitudinal Strain	-1.943	2.279×10^{18}	0.072
	Transvers Strain	-1.899	2.283×10^{18}	0.066
Zigzag Model 9-Rings	Strain-Free	-5.300	1.610×10^{18}	2.402
	Longitudinal Strain	-5.270	1.613×10^{18}	3.038
	Transvers Strain	-5.230	1.613×10^{18}	2.421
Zigzag Model 11-Rings	Strain-Free	-5.105	1.385×10^{18}	4.878
	Longitudinal Strain	-5.069	1.379×10^{18}	5.449
	Transvers Strain	-5.052	1.379×10^{18}	5.363
Zigzag Model 13-Rings	Strain-Free	-4.591	1.204×10^{18}	8.545
	Longitudinal Strain	-4.591	1.204×10^{18}	3.828
	Transvers Strain	-4.570	1.205×10^{18}	4.060

a) Electron rest mass

TABLE III. GAUGE FACTORS OF THE GRAPHENE MODELS.

Model Type		Gauge factor	
		Longitudinal strain	*Transvers strain*
Armchair Model	9 -Rings	-4.64	-6.88
	13-Rings	2.82	-6.05
Zigzag Model	9-Rings	26.28	0.63
	11-Rings	12.21	10.43
	13-Rings	-55.21	-52.50

CONCLUSION

In this paper, the orientation dependence of piezoresistivity in graphene nanoribbons has been discussed by carrying out the first-principles simulation we have originally developed [10, 11]. For the armchair-oriented model series, band structures hardly change due to any strain, and the gauge factors are small as the common characteristics for the armchair-oriented graphene nanoribbons. On the other hand, various values of gauge factors have been obtained according to model size for the zigzag-oriented model series because of the nonuniformity of band structures among the model series. Generally, the zigzag model series have sufficiently large values of gauge factors for practical application to nanoscale piezoresistor. It is expected that zigzag-oriented graphene nanoribbons will have potential for use in future MEMS/NEMS technology.

ACKNOWLEDGMENT

This research is conducted as the Bilateral Joint Research Project funded by Science and Technology Development Fund (STDF) in Egypt and Japan Society for the Promotion of Science (JSPS). The first author also gratefully acknowledges the Mission Sector-MOHE for granting him a scholarship for the Ph.D. degree and Japan International Cooperation Agency (JICA) for their supports through this work.

REFERENCES

[1] E. J. Wilson, "STRAIN-GAGE INSTRUMENTATION," Shock and vibration handbook, 1976.

[2] H. Rolnick, "Tension coefficient of resistance of metals," Physical review, vol. 36, p. 506, 1930.

[3] J. W. Cookson, "Theory of the piezo-resistive effect," Physical review, vol. 47, p. 194, 1935.

[4] A. A. Barlian, W.-T. Park, J. R. Mallon, A. J. Rastegar, and B. L. Pruitt, "Review: Semiconductor piezoresistance for microsystems," Proceedings of the IEEE, vol. 97, pp. 513-552, 2009.

[5] C. S. Smith, "Piezoresistance effect in germanium and silicon," Physical review, vol. 94, p. 42, 1954.

[6] A. K. Geim and K. S. Novoselov, "The rise of graphene," Nature materials, vol. 6, pp. 183-191, 2007.

[7] Y. Lee, S. Bae, H. Jang, S. Jang, S.-E. Zhu, S. H. Sim, Y. I. Song, B. H. Hong, and J.-H. Ahn, "Wafer-scale synthesis and transfer of graphene films," Nano letters, vol. 10, pp. 490-493, 2010.

[8] X. Zheng, X. Chen, J.-K. Kim, D.-W. Lee, and X. Li, "Measurement of the gauge factor of few-layer graphene," Journal of Micro/Nanolithography, MEMS, and MOEMS, vol. 12, pp. 013009-013009, 2013.

[9] G. Mohammed, N. Koichi, F. E.-B. Ahmed MR, T. Osamu, and E.-M. Ahmed Abd, "Simulation of Graphene Piezoresistivity Based on Density Functional Calculations," Modeling and Numerical Simulation of Material Science, vol. 3, p. 117, 2013.

[10] K. Nakamura, Y. Isono, T. Toriyama, and S. Sugiyama, "Simulation of piezoresistivity in n-type single-crystal silicon on the basis of the first-principles band structure," Physical Review B, vol. 80, p. 045205, 2009.

[11] K. Nakamura, Y. Isono, and T. Toriyama, "First-Principles Study on Piezoresistance Effect in Silicon Nanowires," Jpn. J. Appl. Phys, vol. 47, pp. 5132–5138, 2008.

[12] G. Kresse and J. Hafner, "Ab initio molecular dynamics for liquid metals," Physical Review B, vol. 47, p. 558, 1993.

[13] G. Kresse and J. Furthmüller, "Efficient iterative schemes for ab initio total-energy calculations using a plane-wave basis set," Physical Review B, vol. 54, p. 11169, 1996.

[14] P. Hohenberg and W. Kohn, "Inhomogeneous electron gas," Physical review, vol. 136, p. B864, 1964.

[15] J. P. Perdew and Y. Wang, "Accurate and simple analytic representation of the electron-gas correlation energy," Physical Review B, vol. 45, p. 13244, 1992.

[16] J. P. Perdew, J. Chevary, S. Vosko, K. A. Jackson, M. R. Pederson, D. Singh, and C. Fiolhais, "Atoms, molecules, solids, and surfaces: Applications of the generalized gradient approximation for exchange and correlation," Physical Review B, vol. 46, p. 6671, 1992.

[17] D. Vanderbilt, "Soft self-consistent pseudopotentials in a generalized eigenvalue formalism," Physical Review B, vol. 41, p. 7892, 1990.

[18] R. Heyrovska, "Atomic structures of graphene, benzene and methane with bond lengths as sums of the single, double and resonance bond radii of carbon," arXiv preprint arXiv:0804.4086, 2008.

[19] J. P. Lu, "Elastic properties of carbon nanotubes and nanoropes," Physical review letters, vol. 79, p. 1297, 1997.

[20] M. Treacy, T. Ebbesen, and J. Gibson, "Exceptionally high Young's modulus observed for individual carbon nanotubes," 1996.

[21] A. Krishnan, E. Dujardin, T. Ebbesen, P. Yianilos, and M. Treacy, "Young's modulus of single-walled nanotubes," Physical Review B, vol. 58, p. 14013, 1998.

[22] V. Barone, O. Hod, and G. E. Scuseria, "Electronic structure and stability of semiconducting graphene nanoribbons," Nano letters, vol. 6, pp. 2748-2754, 2006.

[23] M. Y. Han, B. Özyilmaz, Y. Zhang, and P. Kim, "Energy band-gap engineering of graphene nanoribbons," Physical review letters, vol. 98, p. 206805, 2007.

[24] C. Kittel, Introduction to Solid State Physics, 8th ed. New York: Wiley, 2005.

[25] J. M. Ziman, Principles of the Theory of Solids, 2nd ed. New York: Cambridge University Press, 1972.

[26] K. Nakamura, Y. Isono, T. Toriyama, and S. Sugiyama, "First-principles simulation on orientation dependence of piezoresistance properties in silicon nanowires," Jpn J Appl Phys, vol. 48, pp. 06FG09-06FG09-5, 2009.

[27] K. Nakamura, T. Toriyama, and S. Sugiyama, "First - Principles Simulation on Piezoresistive Properties in Doped Silicon Nanosheets," IEEJ Transactions on Electrical and Electronic Engineering, vol. 5, pp. 157-163, 2010.

[28] K. Nakamura, T. Toriyama, and S. Sugiyama, "First-principles simulation on thickness dependence of piezoresistance effect in silicon nanosheets," Japanese Journal of Applied Physics, vol. 49, 2010.

[29] K. Nakamura, T. Toriyama, and S. Sugiyama, "First-Principles Simulation on Piezoresistivity in Alpha and Beta Silicon Carbide Nanosheets," Japanese Journal of Applied Physics, vol. 50, 2011.